Computational Materials Science 187 (2021) 110083

Contents lists available at ScienceDirect

Computational Materials Science

journal homepage: www.elsevier.com/locate/commatsci

Temperature-dependent brittle-ductile transition of α-graphyne nanotubes under uniaxial tension

Cun Zhang [a,e,f], Bolin Yang [b], Chao Wang [c], Jinxi Liu [a,e], Wenjie Feng [e,f], Xueqian Fang [a,e,f], Shaohua Chen [b,d,*]

[a] State Key Laboratory of Mechanical Behavior and System Safety of Traffic Engineering Structures, Shijiazhuang Tiedao University, Shijiazhuang 050043, China
[b] Institute of Advanced Structure Technology, Beijing Institute of Technology, Beijing 100081, China
[c] LNM, Institute of Mechanics, Chinese Academy of Sciences, Beijing 100190, China
[d] Beijing Key Laboratory of Lightweight Multi-functional Composite Materials and Structures, Beijing Institute of Technology, Beijing 100081, China
[e] Hebei Key Laboratory of Smart Materials and Structures Mechanics, Shijiazhuang Tiedao University, Shijiazhuang 050043, China
[f] Department of Engineering Mechanics, Shijiazhuang Tiedao University, Shijiazhuang 050043, China

ARTICLE INFO

Keywords:
α-Graphyne nanotube
Brittle-ductile transition
Mechanical property
Temperature
Atomic structure evolution

ABSTRACT

As a novel one-dimensional full-carbon allotrope, the tensile property of α-graphyne nanotubes (α-GNTs) under different temperatures was studied with the reactive molecular dynamics method. A very interesting phenomenon of temperature-dependent brittle-ductile transition for carbon nanomaterials was found no matter what the chirality of the α-GNT is. The α-GNT shows a brittle behavior with an ultimate strain of ~0.2 at relatively low temperatures. When the temperature is higher than a critical temperature, it exhibits a ductile behavior with an ultimate strain of ~0.4. The ultimate strain first decreases and then increases with the increase of temperature. The fundamental mechanism of such a brittle-ductile transition phenomenon was first revealed, which is mainly due to the thermal activation energy-controlled microstructure evolution. Beyond the critical temperature, the atomic structures around some hexagonal corners in α-GNTs would recombine through the continuous formation and annihilation of some new triangular structures. Such a mechanism is totally different from the Stone-Wales defect-induced brittle-ductile transition mechanism in carbon nanotubes (Nardelli et al, Phys. Rev. Lett, 1998, 81 (21): 4656). The influence of temperature on the other physical parameters of α-GNTs, such as the Young's modulus, yield strength, ultimate stress, was also systematically studied. The results in this paper, especially the brittle-ductile transition mechanism, would be of great help to the subsequent study and application of α-GNTs.

1. Introduction

Carbon nanomaterials, for example, fullerenes [1], carbon nanotubes (CNTs) [2], carbon nanoscrolls [3], grapheme [4], have fascinated great attention in the past years, due to their extraordinary mechanical, chemical, electronic properties, and corresponding promising applications. Recently, graphynes (GYs) [5], another full-carbon allotropes with a high degree of *sp* and sp^2 hybridization, have attracted tremendous interests and great progresses have been made in its applications [6–18] since the first synthesis of GY by Li et al. [19] in 2010. Inspired by the discovery of CNTs, graphyne nanotubes (GNTs) first predicted by Coluci et al. [20] in 2003, have also been successfully synthesized by Li et al. [21] in 2011. GNTs, for example, α-, β-, γ-GNTs, etc, can be regarded as seamless cylindrical graphyne sheets [5,22], which inherit diverse geometrical structures and corresponding properties of GYs [22–35].

α-GNTs have the same hexagonal geometrical structures as CNTs, except for the insertion of acetylenic linkages (—C≡C—). It was found in previous studies that such a geometrical similarity would lead to a similar electronic property of α-GNTs to CNTs. For example, DFT calculation [36] shows that all zigzag α-GNTs are semiconductors and the armchair ones would translate from semiconductors into conductors with the increase of tube diameter. The band gaps of α-GNTs show oscillatory behaviors similar to CNTs [37]. Karami and Majidi [38] also report similar chirality dependent electronic properties of α-GNTs. On the other hand, the introduction of acetylenic linkages results in the reduction of the mechanical performance [39], such as the Young's modulus, ultimate stress, as well as thermal conductivity [40] of α-GNTs, in comparison with CNTs.

* Corresponding author.
E-mail address: chenshaohua72@hotmail.com (S. Chen).

https://doi.org/10.1016/j.commatsci.2020.110083
Received 14 March 2020; Received in revised form 15 September 2020; Accepted 27 September 2020
Available online 8 October 2020

Many studies have shown that CNTs have plastic behavior under tension [41–45]. A recent interesting study reports that α-GNTs would have super-plastic behavior under torsion, whose torsional fracture angle is up to 35 times higher than that of CNTs [46]. Do α-GNTs have plastic, ever super-plastic behavior under uniaxial tension? What is the effect of chirality and temperature on the tensile property of α-GNTs?

To address these problems, the effect of the chirality and temperature on the mechanical property of α-GNTs under tension was systematically investigated in this paper using reactive molecular dynamics methods. It is found that, no matter what the chirality is, α-GNTs exhibit a temperature-dependent brittle-ductile transition behavior. The fundamental mechanism of such a new phenomenon was analyzed through dynamic trajectory analysis. The effect of temperature on the Young's modulus, yield strength, yield strain, and ultimate stress of α-GNTs was further achieved. The results provide a deep understanding of the mechanical property of α-GNTs under tension. It should be useful for the subsequent study and future applications of such a novel low-dimensional material.

2. Computational methods

The geometrical structure of α-graphyne sheet (α-GY) [5] and three representative α-GNTs [20], i.e., armchair (9,9), chiral (12, 1) and zigzag (15, 0), are shown in Fig. 1. The structural similarity of α-GY and graphene facilitates a comparison between α-GNTs and CNTs. Construction of zigzag, armchair, and other chiral α-GNTs could be realized analogously to CNTs [5,47]. The commonly used nomenclature (n, m) for CNTs can also be adopted for α-GNTs, as shown in Fig. 1. The GNTs with chiral angles ranging from 0 to $\pi/6$ were systematically investigated in this study, and the detailed information such as tube diameters, lengths, and the temperatures are listed in Table S1 of Supporting materials.

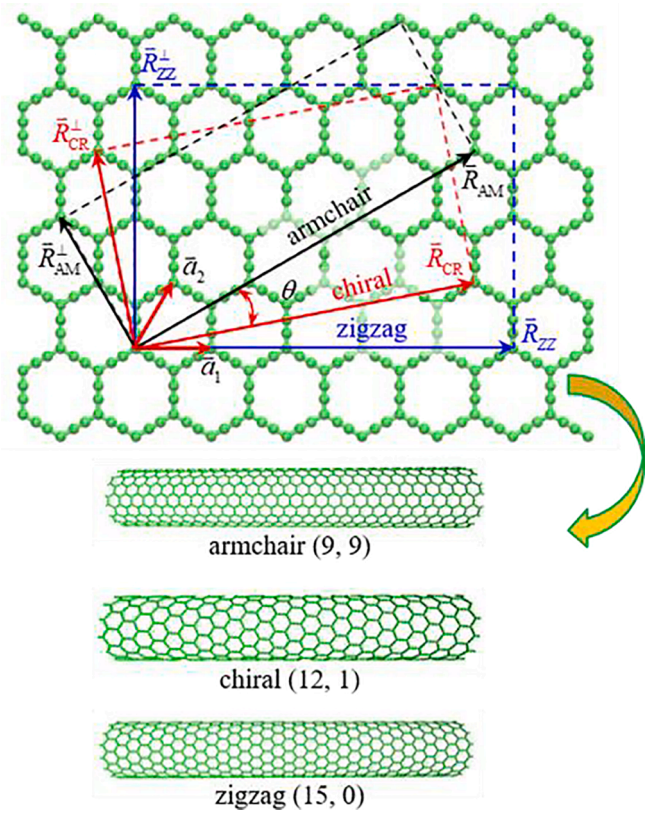

Fig. 1. α-GY and three typical α-GNTs. The geometrical structure of α-GY and the definition of chirality are shown, where $\vec{a}_1$ and $\vec{a}_2$ are lattice vectors of α-GY. θ denotes the chiral angle. Three representative α-GNTs are given with chiralities of (9, 9), (12, 1), (15, 0), respectively.

In previous literature, the ReaxFF forcefield [48,49] was as common as the AIREBO potential [50,51] to study the bond formation and breakage of graphyne nanomaterials. But considering our previous successful application of the AIREBO potential on carbon nanomaterials [52,53], the AIREBO potential [54] was adopted to describe C–C interactions in α-GNTs. The cutoff radius for C–C bonds in the AIREBO potential was increased from 1.7 Å to 2.0 Å to avoid spuriously high bond forces or unphysical results near the fracture region [55].

All simulations were carried out using LAMMPS (Large-scale Atomic/Molecular Massively Parallel Simulator) [56] with periodic boundary conditions (PBC). For each case, α-GNT was firstly optimized using the CG (Conjugate Gradient) method, then relaxed in the NPT ensemble (constant number of atoms, constant pressure, and constant temperature) for 100.0 ps, until it reaches the dynamic stable state under determined temperatures. After that, α-GNT was pulled uniformly along its axial direction at a constant strain rate of 5.0×10^{-5} ps^{-1} in the NVT (constant number of atoms, volume, and temperature) ensemble. The determined temperature was controlled using the Nose-Hoover thermostat [57]. The time step was 1.0 fs and snapshots were recorded per 1.0 ps, which were further analyzed with the VMD visualization package [58]. The atom stress was calculated using viral theorem expressed in the following equation:

$$\sigma_i^{\alpha\beta} = \frac{1}{\Omega_i}\left(- m_i v_i^{\alpha} v_i^{\beta} + \frac{1}{2}\sum_{j \neq i} F_{ij}^{\alpha} r_{ij}^{\beta} \right) \quad (1)$$

where Ω_i, m_i,v_i, represent volume, mass, and velocity of atom i, $F_{ij}^{\alpha\beta}$, $r_{ij}^{\alpha\beta}$, are the force and displacement vector of atom i from atom j. α and β represent the Cartesian coordinate components. The thickness of 3.35 Å of GNTs was adopted according to the previous study [51]. The atom stress was averaged through all atoms and every 100 timesteps to obtain the stress–strain relation.

3. Results and discussions

3.1. Brittle-ductile transition phenomena of α-GNTs

The tensile stress–strain relation for a typical (12, 1) α-GNT under different temperatures is shown in Fig. 2a. Fig. 2a clearly shows that the fracture behavior of α-GNTs can be divided into two types: (a) brittle fracture when the temperature is as low as about 400 K and (b) ductile fracture when the temperature is larger than 500 K. Obviously, a critical brittle-ductile transition temperature should exist between 400 K and 500 K. Further calculations reveal that the critical temperature is about 460 K (See Fig. S1 of Supporting materials). The ultimate strain varying with temperature is given in Fig. 2b. It is found that the ultimate strain decreases slowly with the increase of temperature when less than 460 K and increases monotonically with the increase of temperature when larger than 460 K. When the temperature reaches 700 K, the increasing ultimate strain begins to oscillate around a mean value of 0.35. For comparison, the ultimate stress varying with temperature is given in Fig. 2c, in which the ultimate stress decreases almost linearly with the increase of temperature.

Such a brittle-ductile transition has also been reported for CNTs [41], but with a much smaller ductile strain (<6%) than that of the present α-GNTs (near 40%). The brittle-ductile transition is due to the Stone-Wales defects for CNTs. What is the fundamental mechanism for the brittle-ductile transition and high ductility of α-GNTs?

The morphology evolution of the (12, 1) α-GNT stretching at different temperatures is shown in Fig. 3. A very interesting finding is that a new non-18 atomic ring structure was formed during high temperature stretching. Before the structural fracture, the α-GNT keeps the original ring structure of 18 atoms until failure at 100 K as shown in Fig. 3a. At a higher temperature, 700 K as an example shown in Fig. 3b,

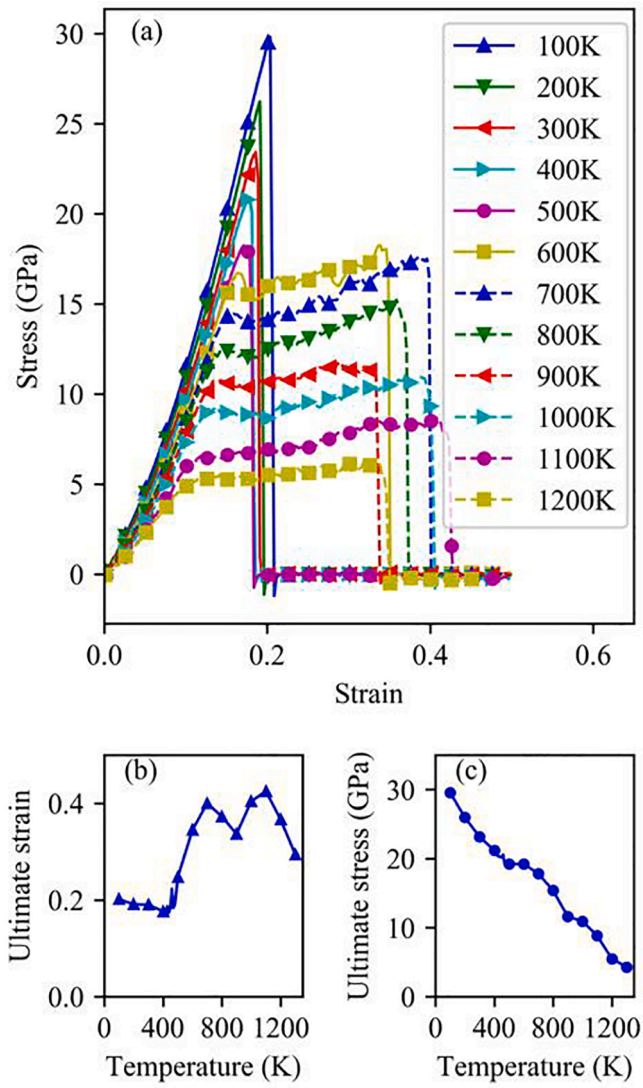

Fig. 2. Tensile behavior of a (12, 1) α-GNT under different temperatures. (a) The stress–strain relation; (b) The ultimate strain varying with temperature; (c) The ultimate stress varying with temperature.

many non-18 atomic ring structures were formed during stretching. By comparing the structural morphology at 700 K and 1000 K, it is found that the higher the temperature is, the more non-18-atom rings can be formed at the same strain; and the smaller the strain is to produce the first non-18-aotm ring. The corresponding dynamic evolution processes at these three temperatures (100 K, 700 K, and 1100 K) are also shown in Movie S1-S3 of Supporting materials. Such a structural evolution of these non-18-atom rings was consistent with the previous study about the torsional superplasticity of α-GNT done by de Sousa et al. [46].

Is the super-ductile behavior of the (12, 1) α-GNT related with the new forming non-18 atomic ring structures? Snapshots of local enlargement of the internal atomic structure were given in Fig. 4, where the structural evolution process of two representative neighboring 18 atomic ring structures during stretching at 700 K is taken as an example. Initially, the two neighboring 18 atomic ring structures (Ring A and Ring B) were marked red and purple, respectively, except for the atoms on the common side, which were labeled yellow. As the external tensile strain increases, the atomic structure deforms. At $\varepsilon = 0.136$, Ring A was stretched but still retains its original 18 atomic ring structure. However, two new triangular structures (rings of 3 atoms) were formed at the top and bottom corner points of Ring B, inducing Ring B a 16 atomic structure. At $\varepsilon = 0.145$, the triangular structure above Ring B disappears

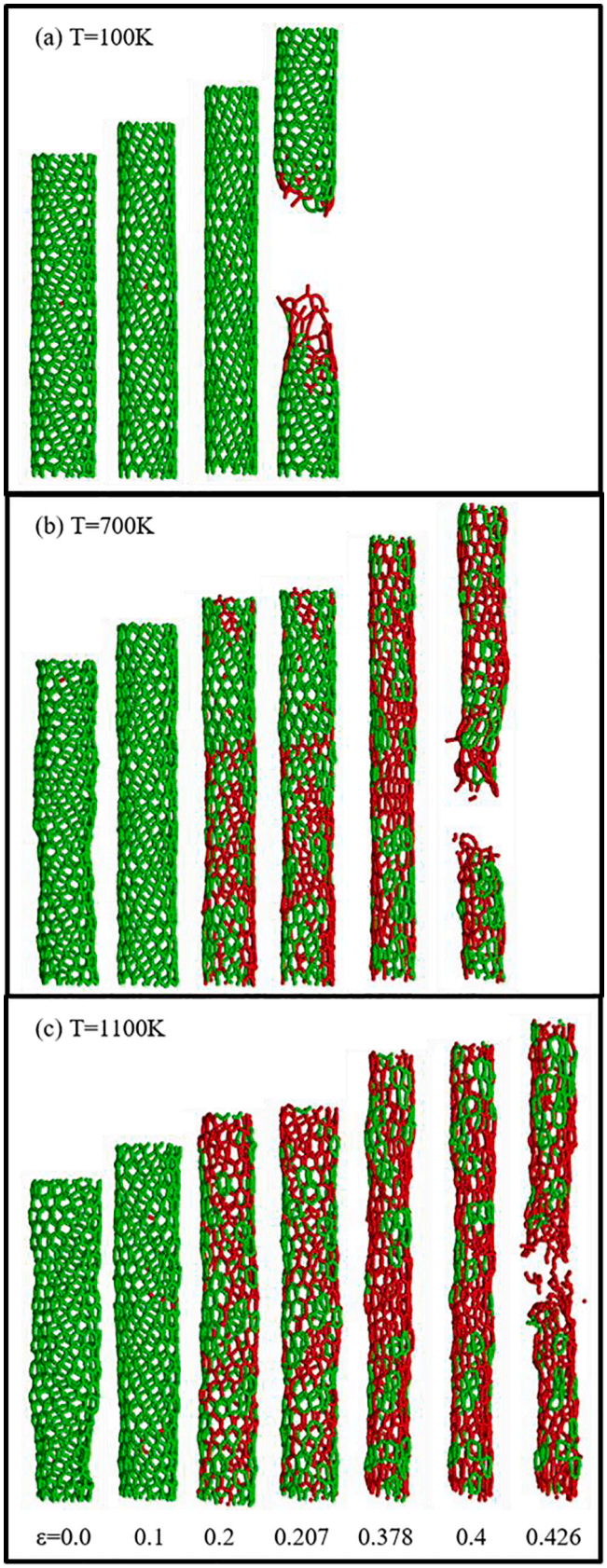

Fig. 3. The structural evolution of a (12, 1) α-GNT at (a) T = 100 K, (b) T = 700 K and (c) T = 1100 K. The ring structure of 18 atoms and the new non-18 atomic ring structure are marked green and red, respectively. The dynamic evolution processes during tension at 100 K, 700 K, and 1100 K are shown in Movie S1-S3 of Supporting materials.

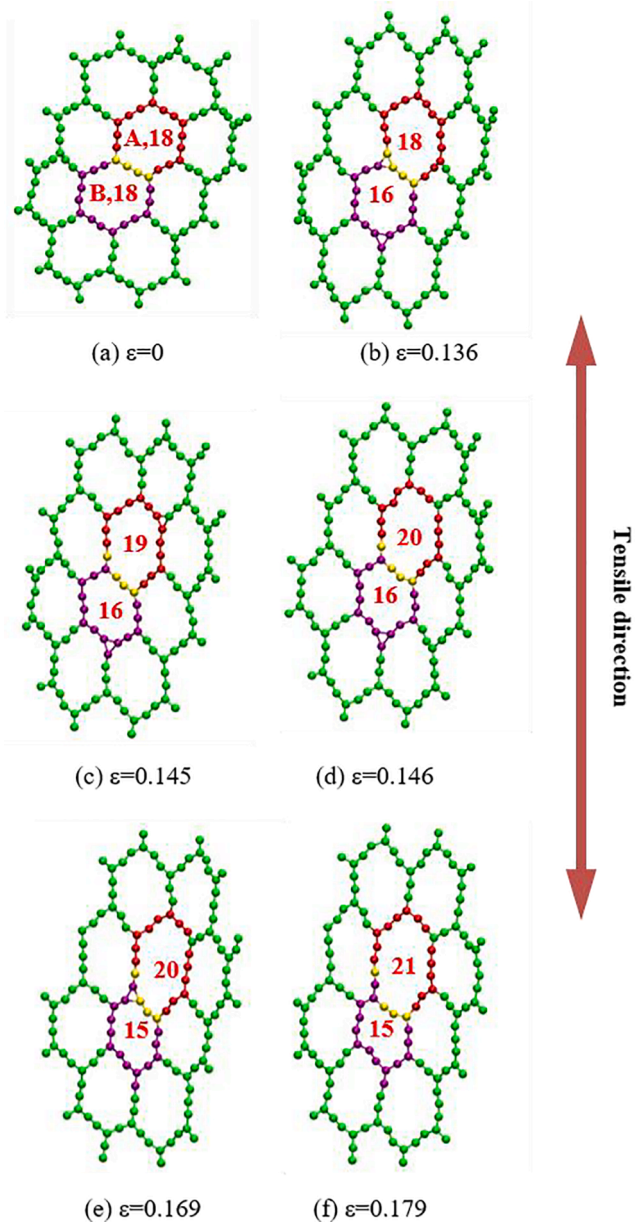

Fig. 4. The structure evolution of two representative neighboring 18-atom-ring structures under tension at 700 K. The upper and lower 18-atom rings, A and B, are marked as red, and purple, respectively, except for their neighbor atoms which are marked as yellow. The atoms surrounding them are marked as green. The dynamic evolution processes during tension are shown in Movie S4 of Supporting materials.

due to the C—C bond breaking, but a new triangular structure forms simultaneously at the upper-right corner of Ring A. As a result, Ring A becomes a 19 atomic structure and Ring B becomes a 16 atomic structure. When the tensile strain increases slightly, i.e., at $\varepsilon = 0.146$, the triangular structure at the upper-right corner of Ring A disappears very soon, leading to a 20 atomic structure of Ring A. At $\varepsilon = 0.169$, the triangular structure below Ring B disappears, but a new triangular structure was formed above Ring B, leading to a 15 atomic structure of Ring B. Through the continuous formation and annihilation of triangular structures, the original 18 atomic structures were gradually reorganized into ring structures with more or fewer atoms. Furthermore, it is found that, during the reorganization, the ring structure deforms and was stretched, but the atomic bonds barely deform, allowing the α-GNT to deform greatly. The Electronic supplementary material provides a Movie S4 for the above evolution process. The C—C bond length variation with tensile strain was analyzed in Fig. S2 of Supporting materials, it was found that during the plastic stage, the bond length barely changed. To evaluate the energy barrier from the formation and annihilation of the carbon triangles, nudged elastic band (NEB) calculations ware performed. It can be found that, with the strain increasing, the energy barrier becomes smaller and smaller. More details about the bond length variation analysis and NEB analysis can be found in Section S3 and S4 of Supporting materials.

Obviously, these triangles and subsequent non-18-atom rings are very important to the superplastic behavior of the α-GNT. Therefore, the number of several representative rings of N atoms (N = 3, 17, 19, 20) varying with the tensile strain at different temperatures was further analyzed, as shown in Fig. 5. The yield point and fracture point of the (12, 1) α-GNT were marked as hollow circles and squares, respectively. It is found that the (12, 1) α-GNT exhibits plastic property when the non-18 atomic ring structures achieve a certain number at a relatively high temperature. However, at a low temperature such as 100 K, non-18 atomic rings can hardly be observed. It should be easy to understand such a result since the atomic structure reconstruction needs the activation energy. At a low temperature, the thermal activation energy is not enough to induce the reconstruction of triangle structures. While, at a relatively high temperature such as 700 K and 1100 K shown in Fig. 5, enough thermal activation energy can be provided to reconstruct the atomic structures, and the higher the temperature is, the earlier the yield

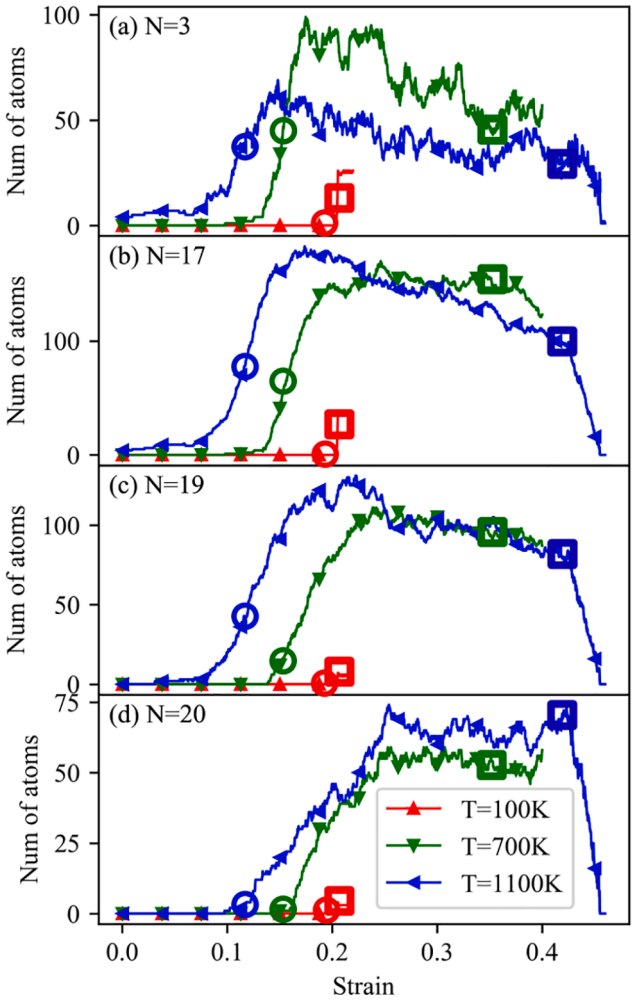

Fig. 5. The number of representative rings of N atoms (N = 3, 17, 19, 20) varying with the tensile strain at different temperatures. The hollow circle and square represent the yield point and fracture point, respectively.

point emerges.

Variation of the potential energy of several representative atoms in the (12,1) α-GNT under stretching at a high temperature, for example, 700 K, is further given in Fig. 6, in which the corresponding local structure evolution is shown as the inset. It shows that the energy of the involved representative atoms changes with the formation and annihilation of the triangular structures. The bond reforming-breaking-reforming behavior through triangular structures would induce bond slipping and plastic behavior [52,53]. The bond slipping would furthermore lead to the large structure deformation of the α-GNT. Meanwhile, the variation of these C–C bond lengths in the α-GNT can be negligible. By comparison, at a low temperature, the thermal activation energy is not enough to produce enough triangle structures or induce bond slipping. Such a special brittle-ductile transition mechanism gives α-GNTs better ductile performance than CNTs at high temperatures.

3.2. Effect of chirality on the brittle-ductile transition of the α-GNTs

Considering the importance of chirality on the carbon nanomaterials [45,59], more than 600 cases (49 chiralities belonging to 10 different chiral angles, 13 temperatures from 100 K to 1300 K with an interval of 100 K for each chirality) were chosen to study the effect of chirality on the brittle-ductile transition of the α-GNT. More details can be found in Section S2 of Supporting materials. It is found that α-GNTs of different chiral angles follow the same brittle-ductile transition mechanism as that of the (12, 1) α-GNT. The critical brittle-ductile transition temperatures (BDTTs) were further given in Fig. 7 for α-GNTs with these 10 chiral angles ranging from 0° (zigzag) to 30° (armchair). It is found that the BDTTs vary from ~360 K to ~900 K with the chiral angles irregularly. But it is still unclear why they fluctuate so largely with the chiral angles.

3.3. Effect of temperature on the mechanical properties of α-GNTs

The mechanical properties of α-GNTs influenced by temperature were also investigated. Plenty of calculations have been carried out (for detailed information about these simulations, see Table S1 of Supporting materials) and it is found that the relationship between the stress and strain of different chiral α-GNTs is similar to that of the (12, 1) α-GNT shown in Fig. 2a. At low temperatures, all α-GNTs exhibit an approximately linear stress–strain relationship until brittle fracture. At high temperatures, all α-GNTs exhibit an approximately linear elasticity and then plasticity until ductile fracture. The Young's modulus of three representative α-GNTs varying with the temperature is given in Fig. 8, where it shows a decreasing Young's modulus with the increase of temperature. Here, the Young's modulus of each α-GNT is defined as the initial slope of the stress–strain curve with a sufficient small strain

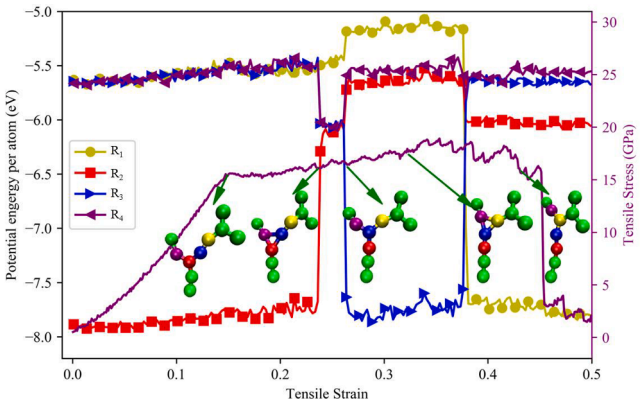

Fig. 6. The potential energy of representative atoms in a (12, 1) α-GNT varying with the tensile strain at 700 K. Symbols of different colors represent atoms of the corresponding color.

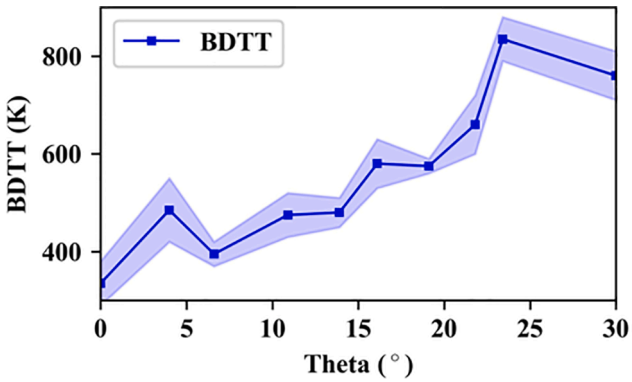

Fig. 7. The critical brittle-ductile transition temperature (BDTT) varying with the chiral angle of α-GNTs. The 10 points and the colored area are corresponding to the mean and variance of these BDTTs of theseα-GNTs with the same chiral angles.

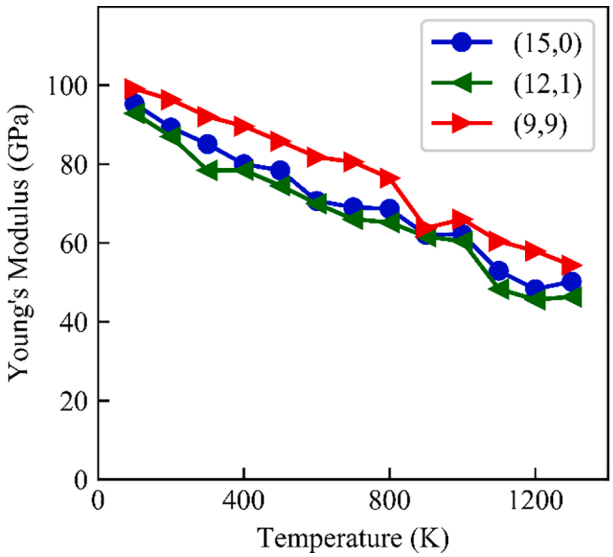

Fig. 8. The effect of temperature on the Young's modulus of three representative α-GNTs.

(<5%).

The effect of temperature on the yield stress, yield strain, ultimate stress, and ultimate strain of three representative α-GNTs is given in Fig. 9. As shown in Fig. 9(a)-9(c), the yield stress, yield strain, and ultimate stress decrease monotonically with the increase of temperature. However, the varying trend of ultimate strain is influenced by the critical brittle-ductile transition temperature as shown in Fig. 9(d). When the temperature is less than the critical brittle-ductile transition one, the ultimate strain decreases with the increase of temperature. When the temperature is greater than the critical brittle-ductile transition temperature, the ultimate strain increases with the increase of temperature. It should be noticed that, with the temperature further increasing, α-GNTs show a decreasing ultimate strain. This is because the C–C bond breaks ahead of time at high temperatures due to the large enough thermal activation energy.

4. Conclusions

The tensile property of α-GNTs was systematically studied with the reactive molecular dynamics method. It is found that the mechanical property of α-GNTs is controlled by a critical temperature: (1) below the critical temperature, the α-GNT exhibits linear elasticity and brittle

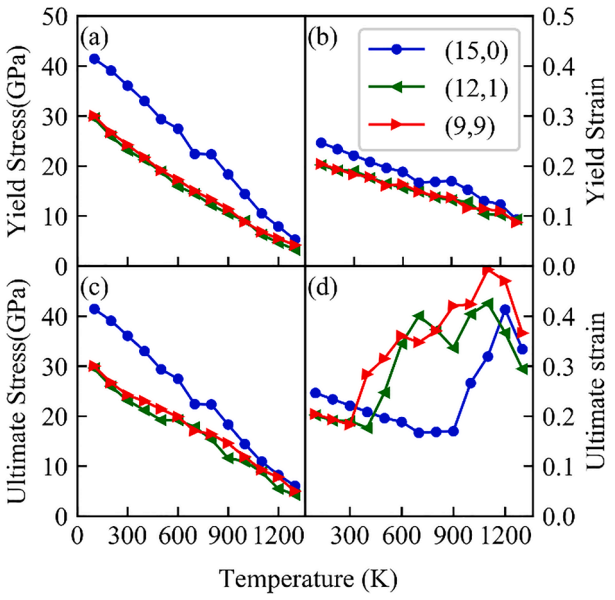

Fig. 9. Temperature effect on the yield stress, yield strain, ultimate stress, and ultimate strain of three representative chiral GNTs.

fracture; (2) beyond the critical temperature, it exhibits elastic–plastic behavior and ductile fracture. The ultimate strain of an elastic–plastic α-GNT can exceed that of CNT by about 6 times. Such a brittle-ductile transition is due to the thermal activation energy-controlled microstructure evolution. Under the action of sufficient thermal activation energy and tensile strain, the original 18-atomic ring structures in α-GNTs deform and then continuously recombine to form new ring structures of more or fewer atoms, through the continuous formation and annihilation of some new triangular structures. This interesting behavior is independent of the chirality of α-GNTs. The material parameters of α-GNTs, including the Young's modulus, yield stress, and ultimate stress decrease with the increase of temperature, while the ultimate strain would decrease first when the temperature is less than the critical brittle-ductile transition temperature, and then increase when the temperature is beyond the critical one. The results in the present paper give a new brittle-ductile transition mechanism for α-GNTs, which should be useful to the application and further research of α-GNTs.

CRediT authorship contribution statement

Cun Zhang: Conceptualization, Methodology, Software, Validation, Data curation, Investigation, Writing - original draft, Writing - review & editing. **Bolin Yang:** Software, Validation, Data curation, Writing - original draft, Writing - review & editing. **Chao Wang:** Methodology, Writing - original draft, Writing - review & editing. **Jinxi Liu:** Writing - review & editing. **Wenjie Feng:** Writing - review & editing. **Xueqian Fang:** Writing - review & editing. **Shaohua Chen:** Conceptualization, Methodology, Software, Validation, Writing - original draft, Writing - review & editing, Project administration.

Declaration of Competing Interest

The authors declare that they have no known competing financial interests or personal relationships that could have appeared to influence the work reported in this paper.

Acknowledgments

The work reported here is supported by NSFC Grants #11502150, 11532013, 11872114, Natural Science Foundation of Hebei Province (A2016210060), and the Higher Education Youth Talents Program of Hebei Province (BJ2017052).

Appendix A. Supplementary data

Supplementary data to this article can be found online at https://doi.org/10.1016/j.commatsci.2020.110083, in which LAMMPS input file (in.tension), data file (data.CNT_1201) and modified AIREBO forcefield file (CH.airebo) are also included.

References

[1] H.W. Kroto, J.R. Heath, S.C. O'Brien, R.F. Curl, R.E. Smalley, Nature 318 (1985) 162.
[2] S. Iijima, Nature 354 (1991) 56.
[3] T. Wang, C. Zhang, S. Chen, J. Nanosci. Nanotechnol. 13 (2013) 1136–1140.
[4] K.S. Novoselov, A.K. Geim, S.V. Morozov, D. Jiang, Y. Zhang, S.V. Dubonos, I. V. Grigorieva, A.A. Firsov, Science 306 (2004) 666–669.
[5] R.H. Baughman, H. Eckhardt, M. Kertesz, J. Chem. Phys. 87 (1987) 6687–6699.
[6] H. Shang, Z. Zuo, L. Li, F. Wang, H. Liu, Y. Li, Y. Li, Angew. Chem. Int. Ed. 57 (2018) 774–778.
[7] X. Gao, H. Ren, J. Zhou, R. Du, C. Yin, R. Liu, H. Peng, L. Tong, Z. Liu, J. Zhang, Chem. Mater. 29 (2017) 5777–5781.
[8] H. Shang, Z. Zuo, L. Yu, F. Wang, F. He, Y. Li, Adv. Mater. 30 (2018) 1801459.
[9] R. Matsuoka, R. Sakamoto, K. Hoshiko, S. Sasaki, H. Masunaga, K. Nagashio, H. Nishihara, J. Am. Chem. Soc. 139 (2017) 3145–3152.
[10] K. Wang, N. Wang, J. He, Z. Yang, X. Shen, C. Huang, ACS Appl. Mater. Interfaces 9 (2017) 40604–40613.
[11] Q. Li, C. Yang, L. Wu, H. Wang, X. Cui, J. Mater. Chem. A 7 (2019) 5981–5990.
[12] Z. Zuo, D. Wang, J. Zhang, F. Lu, Y. Li, Adv Mater 31 (2019), 1803762.
[13] J. Saleem, L. Wang, C. Chen, Adv. Healthcare Mater. 7 (2018) 1800525.
[14] X. Gao, H. Liu, D. Wang, J. Zhang, Chem. Soc. Rev. 48 (2019) 908–936.
[15] H. Qiu, M. Xue, C. Shen, Z. Zhang, W. Guo, Adv. Mater. 31 (2019) 1803772.
[16] W. Jiang, Z. Zhang, Q. Wang, J. Dou, Y. Zhao, Y. Ma, H. Liu, H. Xu, Y. Wang, Nano Lett. 19 (2019) 4060–4067.
[17] J. Xu, C. Zhu, Y. Wang, H. Li, Y. Huang, Y. Shen, J.S. Francisco, X.C. Zeng, S. Meng, Nano Res. 12 (2019) 587–592.
[18] J. Xu, H. Jiang, Y. Shen, X.-Z. Li, E.G. Wang, S. Meng, Nat. Commun. 10 (2019) 3971.
[19] G. Li, Y. Li, H. Liu, Y. Guo, Y. Li, D. Zhu, Chem. Commun. 46 (2010) 3256–3258.
[20] V. Coluci, S. Braga, S. Legoas, D. Galvao, R. Baughman, Phys. Rev. B 68 (2003), 035430.
[21] G. Li, Y. Li, X. Qian, H. Liu, H. Lin, N. Chen, Y. Li, J. Phys. Chem. C 115 (2011) 2611–2615.
[22] D.-C. Yang, R. Jia, Y. Wang, C.-P. Kong, J. Wang, Y. Ma, R.I. Eglitis, H.-X. Zhang, J. Phys. Chem. C 121 (2017) 14835–14844.
[23] B. Bhattacharya, N. Singh, R. Mondal, U. Sarkar, Phys. Chem. Chem. Phys. 17 (2015) 19325–19341.
[24] X. Chen, Phys. Chem. Chem. Phys. 17 (2015) 29340–29343.
[25] V. Coluci, D. Galvao, R. Baughman, J. Chem. Phys. 121 (2004) 3228–3237.
[26] Y. Deng, J. Cao, J. Atomic Mol. Phys. 30 (2013) 812–818.
[27] A. Enyashin, Y.N. Makurin, A. Ivanovskii, Carbon 42 (2004) 2081–2089.
[28] M. Hu, Y. Jing, X. Zhang, Phys. Rev. B 91 (2015), 155408.
[29] X.-M. Wang, S.-S. Lu, J. Phys. Chem. C 117 (2013) 19740–19745.
[30] H. Zhao, D. Wei, L. Zhou, H. Shi, X. Zhou, Comput. Mater. Sci. 106 (2015) 69–75.
[31] J. Deb, B. Bhattacharya, D. Paul, U. Sarkar, Physica E 84 (2016) 330–339.
[32] M. Li, Y. Zhang, Y. Jiang, Y. Zhang, Y. Wang, H. Zhou, RSC Adv. 8 (2018) 15659–15666.
[33] H. Pourmirzaagha, A. Yekrangi Sendi, S. Rouhi, Physica E 119 (2020), 114044.
[34] A. Reihani, A. Soleimani, S. Kargar, V. Sundararaghavan, A. Ramazani, J. Phys. Chem. C 122 (2018) 22688–22698.
[35] H. Pourmirzaagha, A.Y. Sendi, S. Rouhi, Physica E (2020), 114044.
[36] B. Kang, J.Y. Lee, Carbon 84 (2015) 246–253.
[37] B. Kang, D. Cho, J.Y. Lee, Phys. Chem. Chem. Phys. 19 (2017) 7919–7922.
[38] R. Majidi, A.R. Karami, Comput. Mater. Sci. 97 (2015) 227–230.
[39] J.M. De Sousa, R.A. Bizao, V.P. Sousa Filho, A.L. Aguiar, V.R. Coluci, N.M. Pugno, E.C. Girao, A.G. Souza Filho, D.S. Galvao, Comput. Mater. Sci. 170 (2019), 109153.
[40] A. Ramazani, A. Reihani, A. Soleimani, R. Larson, V. Sundararaghavan, Carbon 123 (2017) 635–644.
[41] M.B. Nardelli, B.I. Yakobson, J. Bernholc, Phys. Rev. Lett. 81 (1998) 4656.
[42] J. Huang, S. Chen, Z. Wang, K. Kempa, Y. Wang, S. Jo, G. Chen, M. Dresselhaus, Z. Ren, Nature 439 (2006) 281.
[43] C. Tang, W. Guo, C. Chen, Phys. Rev. B 79 (2009), 155436.
[44] C. Tang, W. Guo, C. Chen, Phys. Rev. Lett. 100 (2008), 175501.
[45] T. Chang, J. Geng, X. Guo, Appl. Phys. Lett. 87 (2005), 251929.
[46] J.M. de Sousa, G. Brunetto, V.R. Coluci, D.S. Galvão, Carbon 96 (2016) 14–19.
[47] M. Fujita, R. Saito, G. Dresselhaus, M.S. Dresselhaus, Phys. Rev. B Condens. Matter 45 (1992) 13834–13836.
[48] S.W. Cranford, M.J. Buehler, Carbon 49 (2011) 4111–4121.
[49] B. Faria, N. Silvestre, J.N.C. Lopes, Comput. Mater. Sci. 171 (2020), 109233.
[50] Y. Yang, X. Xu, Comput. Mater. Sci. 61 (2012) 83–88.
[51] Y. Zhang, Q. Pei, C. Wang, Appl. Phys. Lett. 101 (2012), 081909.

[52] C. Zhang, Z. Peng, S. Chen, J. Phys. Chem. C 118 (2014) 19477–19483.
[53] C. Zhang, S. Chen, Nano Res. 8 (2015) 2988–2997.
[54] S.J. Stuart, A.B. Tutein, J.A. Harrison, J. Chem. Phys. 112 (2000) 6472–6486.
[55] S. Wang, Z. Fan, Y. Cui, S. Zhang, B. Yang, H. Chen, Carbon 111 (2017) 486–492.
[56] S. Plimpton, J. Comput. Phys. 117 (1995) 1–19.
[57] W. Shinoda, M. Shiga, M. Mikami, Phys. Rev. B 69 (2004), 134103.
[58] W. Humphrey, A. Dalke, K. Schulten, J. Mol. Graph. 14 (1996) 33–38.
[59] J. Deb, D. Paul, U. Sarkar, P.W. Ayers, J. Mol. Model. 24 (2018) 249.